CrossMark

Solution-processed P3HT-functional graphene for efficient heterojunction organic photoelectronics

Jian Ye[a)]
Department of Chemistry and Environmental Engineering, Bengbu College, Bengbu, Anhui 233030, China

Xueliang Li
Department of Application Chemistry, School of Chemical Engineering, Hefei University of Technology, Hefei, Anhui 230009, China

Jianjun Zhao, Xuelan Mei, and Qian Li
Department of Chemistry and Environmental Engineering, Bengbu College, Bengbu, Anhui 233030, China

(Received 13 January 2016; accepted 9 June 2016)

A facile method that allows chemical functionalization of graphene sheets is described. These result in a solution processable graphene-based material, namely F-graphene, which can be integrated in organic photoelectronic devices, due to its unique structural and photophysical properties. The resultant poly(3-hexylthiophene)(P3HT):F-graphene are soluble in common organic solvents, facilitating the structure/property characterization and the device fabrication by solution processing. The synthesized F-graphene is blended with the conjugated polymer in optimized concentration. The high and sensitive photoresponse of P3HT:F-graphene was demonstrated by the photodetector. A heterojunction photovoltaic device based on the solution-cast P3HT:F-graphene (with a BHJ structure of ITO/ZnO/P3HT:F-graphene/MoO_3/Ag) showed a power conversion efficiency of 1.9% under AM1.5 illumination (100 mW/cm^2). It provides a new method for graphene application in organic photoelectronics. It can easily enhance the performance of devices by optimizing the structure and bulk heterojunction blend in the near future.

I. INTRODUCTION

Organic solar cells (OSCs) offer great technological potential as renewable and alternative sources of electrical energy.[1–6] The possibility of using new organic semiconducting materials in place of silicon wafers in the fabrication of photovoltaic cells provides the prospect of lower manufacturing cost through the employment of various roll-to-roll techniques using solution-processable materials. In the field of organic photovoltaics, bulk heterojunction (BHJ) structures based on interpenetrating networks of conjugated polymers and fullerenes are the most intensely studied. Significant efforts have been applied toward improving the competitive power conversion efficiencies (PCEs) and the long-term air stability of OSCs.[7–9]

The most efficient OSCs have been based on BHJ devices composed of a blend of an electron-donating low-band-gap conjugate polymer such as poly(3-hexylthiophene) (P3HT) and an electron acceptor such as fullerene or a fullerene derivative. Although both small molecules and polymeric materials with low-band-gap energies have been extensively investigated as p-type electron donor materials, not as many electron accepting fullerene derivatives have been actively studied because of difficulties associated with their synthesis. Thus, it is worthwhile to study new type of acceptor with good solubility and optimized energy levels.[10–12]

Novel carbon-based structures, such as carbon nanotubes and graphene, have emerged in recent years as integrative materials for organic photovoltaic devices. The most recent fundamental block of intriguing actual scientific and technological interest is graphene, best described as a two-dimensional (2D) single atom-thick sheet of sp^2 hybridized carbon atoms arranged in a honeycomb lattice with outstanding electronic, mechanical, thermal, and chemical properties. Various graphene materials have been used in OSC devices, especially for interfacial layers.[13–19] However, seldom systematic study has been done on the application of BHJ materials for OSC, due to the poor oil solubility of graphene for the deposition and construction network active layer.

In this paper, a facile method that allows chemical functionalization of graphene sheets is described. These result in a solution processable graphene-based material, namely F-graphene, which can be integrated in organic photoelectronic devices, due to its unique structural and photophysical properties. F-graphene displays increased

Contributing Editor: Sam Zhang
[a)]Address all correspondence to this author.
e-mail: bbyejian@126.com
DOI: 10.1557/jmr.2016.243

 © Materials Research Society 2016

https://doi.org/10.1557/jmr.2016.243 Published online by Cambridge University Press

solubility in common organic solvents as compared to that of the untreated graphene. The synthesized F-graphene is blended with the conjugated polymer poly(3-hexylthiophene), P3HT, in different concentrations. The structure and morphology of the polythiophene–graphene composites are characterized by x-ray diffraction (XRD), scanning electron microscopy (SEM) and transmission electron microscopy (TEM), whereas their spectroscopic properties are investigated by ultraviolet (UV)/vis and Raman spectroscopies. It is demonstrated that utilization of F-graphene in photoelectronic devices exhibits significantly photovoltaic performance, indicating the potential of utilizing a new electron acceptor graphene material.

II. EXPERIMENTAL PROCEDURE

A. Material synthesis

The Synthesis procedure is shown in Fig. 1(a). GO (graphene oxide) were prepared by Hummers' oxidation method,[20] starting from a high-surface-area graphite, 325 mesh (purchased from Nanjing XFNANO Materials Tech). Little quantity (120 mL) of concentrated sulfuric acid and 2.5 g of sodium nitrate was introduced into a 2000 mL three-neck round bottomed flask immersed into an ice bath and 5 g of graphite was added, under nitrogen, with magnetic stirring. After obtaining a uniform dispersion of graphite powders, 15 g of potassium permanganate were added very slowly to minimize or avert possible of explosion. The reaction mixture was thus heated to 35 °C and stirred for 24 h. The resulting dark green slurry was first poured into a copious amount of deionized water, and then centrifuged at 10,000 rpm for 15 min. The isolated GO powder was first washed twice with 100 mL of a 5 wt% HCl aqueous solution and subsequently thoroughly washed with deionized water. It was dried in a vacuum refrigerant dryer for 24 h to obtain GO powder.

1. Function of GO by imidazole

Little quantity (1 g) GO was loaded in a 250 mL round bottom flask and water (100 mL) was added, yielding an inhomogeneous yellow-brown dispersion. This dispersion was sonicated using an ultrasonic bath cleaner (150 W) until it became clear with no visible particulate matter. A mount of imidazole (5 g) was added in the bottom flask. The solution was heated in an oil bath at 118 °C under a water-cooled condenser for 24 h. This product was isolated by filtration over a medium fritted glass funnel, washed copiously with water (5 × 100 mL) and methanol (5 × 100 mL) to wash the residual imidazole, and dried in a vacuum refrigerant dryer for 24 h to obtain functioned-GO (F-GO) powder.

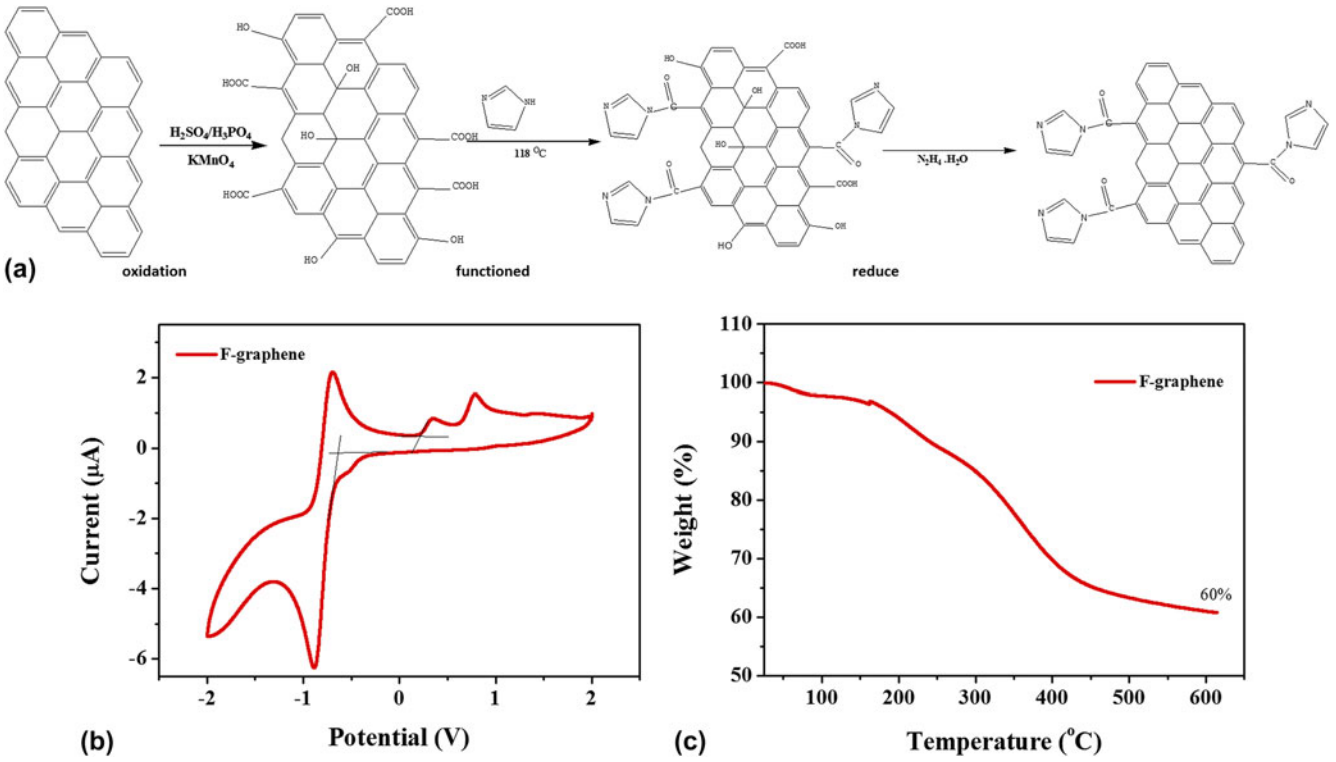


FIG. 1. (a) Synthesis procedure for functionalization of graphene, which involves the imidazole, treatment of pristine graphene. (b) CV of functional graphene drop-cast on a Pt electrode in 0.1 mol/L Bu_4NPF_6 -acetonitrile solutions at a scan rate of 50 mV/s. (c) The TGA weight loss of the functional graphene.

https://doi.org/10.1557/jmr.2016.243 Published online by Cambridge University Press

2. Reduction of F-GO by hydrazine hydrate

The reduction of F-GO by hydrazine hydrate is likely the function of GO. In a typical procedure, F-GO (100 mg) was loaded in a 250 mL round bottom flask and water (100 mL) was then added, yielding an inhomogeneous yellow-brown dispersion. This dispersion was sonicated using an ultrasonic bath cleaner (150 W) until it became clear with no visible particulate matter. Hydrazine hydrate (1.00 mL, 32.1 mmol) was then added and the solution heated in an oil bath at 100 °C under a water-cooled condenser for 24 h over which the reduced F-GO gradually precipitated out as a black solid. This product was isolated by filtration over a medium fritted glass funnel, washed copiously with water (5 × 100 mL) and methanol (5 × 100 mL), and dried in a vacuum refrigerant dryer for 24 h to yield reduced F-GO powder. Here we named the reduced F-GO as F-graphene.

B. Characterizations

TEM imaging was performed on a JEOL JEM-2100F (JEOL Ltd., Tokyo, Japan). SEM imaging was performed on FEI Quanta 200F (FEI Company, Hillsboro, Oregon). TEM samples were prepared in water solution. XRD measurements were performed with a Rigaku D/Max-B x-ray diffractometer (Rigaku Corporation, Tokyo, Japan) with Bragg-Brentano parafocusing geometry, a diffracted beam monochromator, and a conventional cobalt target x-ray tube set to 40 kV and 30 mA. The UV-visible spectra of the samples were recorded on a PerkinElmer Lambda 750 spectrophotometer (PerkinElmer Inc., Waltham, Massachusetts). X-ray photoelectron spectroscopy (XPS) studies were performed on a Thermo-VG Scientific ESCALAB 250 photoelectron spectrometer using a monochromated Al (K_α) (1486.6 eV) x-ray source (Thermo Fisher Scientific, Leicestershire, United Kingdom). The thermogravimetric analysis (TGA) was carried out in N_2 on a TA instrument with a heating rate of 10 °C/min. The atomic force microscopy (AFM) images were recorded on a nanoscope III A scanning probe microscope (Digital Instruments Inc., Tonawanda, New York).

C. Photoelectronics device fabrication

ITO-coated glass substrates were first cleaned by ultrasonic agitation in acetone, detergent, deionized water, and isopropanol sequentially, followed by UV ozone treatment for 15 min. For the cathode buffer layer, ZnO precursor was prepared according to the sol–gel-derived method.[21] Typically, zinc acetate dihydrate ($Zn(CH_3COO)_2{\cdot}2H_2O$, Aldrich, 99.9%, 1 g) and ethanolamine ($NH_2CH_2CH_2OH$, Aldrich, 99.5%, 0.28 g) were dissolved in 2-methoxyethanol ($CH_3OCH_2CH_2OH$, Aldrich, 99.8%, 10 mL) under vigorous stirring for 12 h for the hydrolysis reaction in air. ZnO precursor solution was spin-coated at 4000 rpm for 60 s and then annealed at 200 °C for 1 h. The tetrahydrofuran (THF) solution of P3HT and F-graphene with different ratios was then spin-coated on top of ETL films at 600 rpm for 30 s and 1400 rpm 2 s. After drying for 2 h, the film was annealed at 150 °C for 10 min in N_2-filled glove box. Finally, 7 nm thickness of MoO_3 and Ag (100 nm) were thermally evaporated at a pressure of 4×10^{-4} Pa through a shadow mask to form an active area of ~0.04 cm^2.

III. RESULTS AND DISCUSSION

Data from TGA, are presented in Fig. 1(b). F-graphene displays improved thermal stability until 600 °C. Briefly, TGA curve of F-graphene shows a 3% weight loss before 150 °C, due to humidity and the evaporation of possible remaining solvent. In the range of 150–350 °C, a weight loss of approximately ~20% occurred due to the decomposition of oxygen and isothiocyanate functional groups. From 350 to 600 °C, a weight loss of ~40% was observed, which can be attributed to the removal of the imidazole group. The TGA analysis further confirms that graphene was successfully functionalized.[22] The highest occupied molecular orbit/lowest unoccupied molecular orbital (HOMO/LUMO) energy levels of F-graphene were investigated by cyclic voltammetry (CV) as shown in Fig. 1(c). The HOMO energy level of the polymers was determined from the oxidation onset of the second scan from CV data. It is assumed that the redox potential of Fc/Fc^+ has an absolute energy level of −4.40 eV to vacuum. The energies of the HOMO and LUMO levels were calculated according to the following equations:

$$E_{\mathrm{HOMO}} = -(\Phi_{\mathrm{ox}} + 4.4)(\mathrm{eV})$$

$$E_{\mathrm{LUMO}} = -(\Phi_{\mathrm{red}} + 4.4)(\mathrm{eV}) \quad ,$$

where Φ_{ox} and Φ_{red} are the onset oxidation potential and the onset reduction potential versus Ag/Ag^+, respectively. Introducing oxygen-rich groups around the F-graphene impacts a significant effect on the band gap of the resultant F-graphene. From the value of Φ_{ox} and Φ_{red}, the HOMO and LUMO energy levels F-graphene are about −5.0 and −4.3 eV, respectively. These results can also demonstrate the functionalization of graphene and suggest the use of F-graphene as an acceptor in BHJ devices.[18]

The as-prepared graphene and F-graphene samples were also characterized by XRD, Fig. 2(a). The diffraction peak at $2\theta = 10.8°$ has been attributed to the (002) main reflection of stacks of graphene. The diffractogram of F-graphene does not exhibit the peak at 10.8°; instead peak is observed at 12.5° together with a more prominent one at 24.0°; the former should be attributed to the interplanar spacing of the disordered stacking of functionalized graphene.[23,24] The peak at 24.0° may be due to a partial reduction of F-graphene during the functionalization

https://doi.org/10.1557/jmr.2016.243 Published online by Cambridge University Press

reaction. To further investigate the F-graphene, graphene before and after functionalization exhibits two characteristic peaks at 1352 and 1595 cm^{-1} in Raman spectra [Fig. 2(b)]. These features can be attributed to the D and G peaks of F-graphene, respectively. Compared with pristine graphene, higher intensity of D peaks in F-graphene indicates its enhanced oxidation. The conversion of pristine to F-graphene were also obviously evidenced by the variation of 2D band at ~2650 cm^{-1} from a sharp peak of F-graphene.

Figure 3 shows XPS spectra of graphene before and after functionalization. While Fig. 3(a) shows only the C and O peaks for graphene, the corresponding XPS spectrum for the F-graphene reveals the presence of carbon, oxygen, and nitrogen. Figures 3(b)–3(d) show the different element spectrum for C, N and O, respectively.

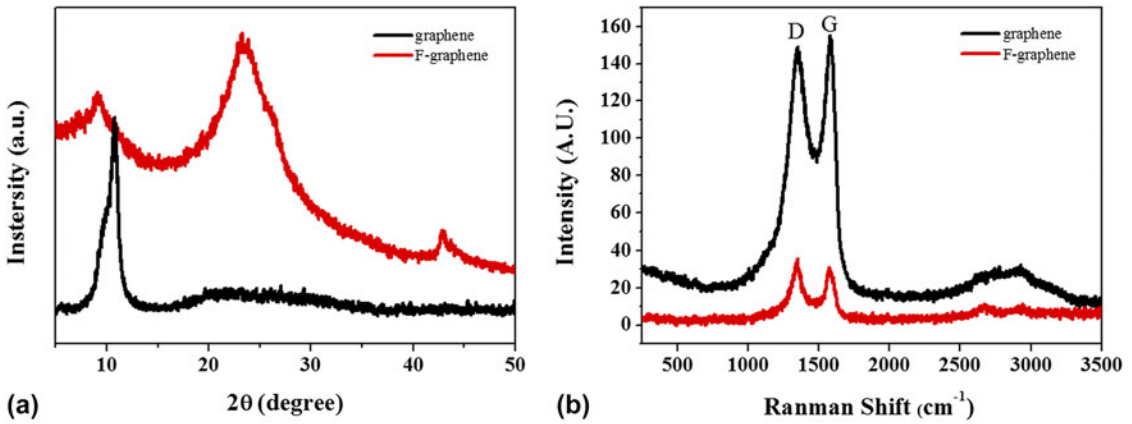


FIG. 2. The (a) x-ray diffusion and (b) Raman spectrum of pristine graphene powders (black line) and functional graphene powders (red line).

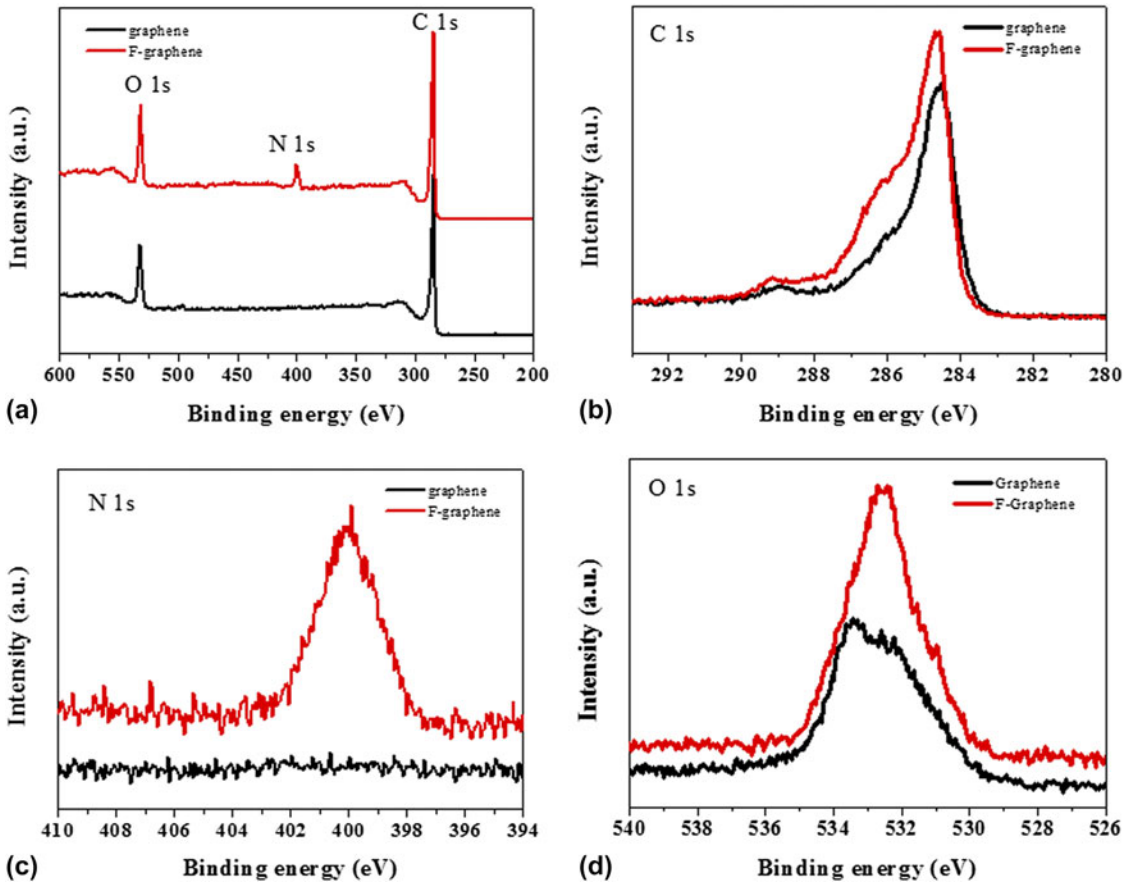


FIG. 3. (a) XPS survey spectra of pristine graphene powders (black line) and functional graphene powders (red line). (b) XPS carbon 1*s* spectra. (c) XPS nitrogen 1*s* spectra. (d) XPS oxygen 1*s* spectra.

https://doi.org/10.1557/jmr.2016.243 Published online by Cambridge University Press

It is clearly found the big improvement of the intensity of C, N, and O peak, especially the N1*s* peak. Moreover, it could be observed that the C peak change from binding energy of 284.5 eV to 285.4 eV and the O peak change from 533.3 eV to 532.4 eV. All above the XPS analysis could prove the functionalization of graphene and also verify the good solubility for F-graphene.[17,19] In addition, to give a more direct evidence of the good solubility for F-graphene, the UV-vis absorption studies of pristine graphene and functional graphene powders in THF solution was carried out (Fig. 4). The standing test for pristine graphene and functional graphene suspension after the ultrasonic treatment can exhibit the solubility. As expected, the UV-vis absorption spectra of pristine graphene suspension have a huge decrease after only 1 h standing, which means massive aggregation of graphene, as shown in Fig. 4(a). The dispersibility of the GO was measured to compare with F-graphene. As shown in Fig. S1, the UV-vis absorption spectra of GO suspension also have a huge decrease after only 1 h standing, attributing to the low dispersibility of GO in THF solution. However, the UV-vis absorption spectra of functional graphene suspension in Fig. 4(b) show a little difference even after difference after as long as 24 h standing.

In order to investigate the morphology of F-graphene, the TEM and SEM were used and the images are shown in Figs. 5 and 6. The pristine graphene exhibits a wrinkled and crinkly structure of aggregation [Figs. 5(a) and 5(b)], with a rough surface [Fig. 6(a)]. It is mainly due to the π–π stacking between the individual graphene layers. However, the TEM images of F-graphene powders show

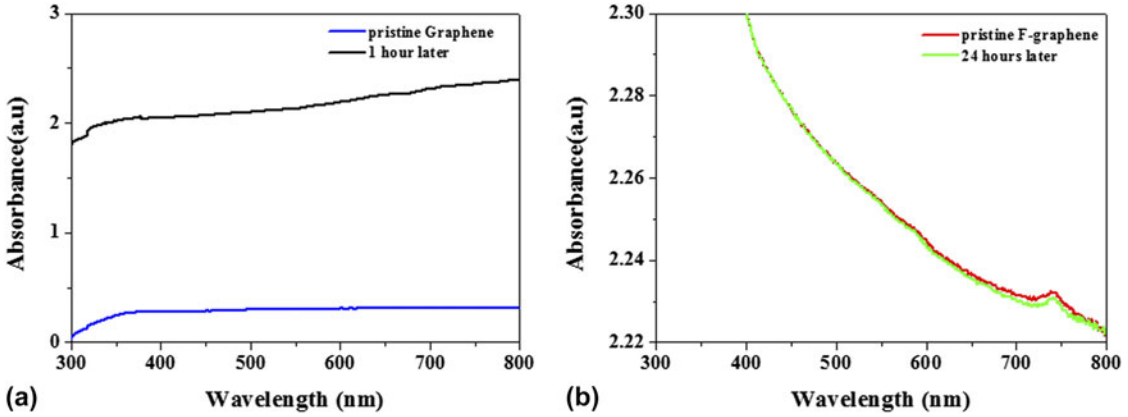


FIG. 4. The absorbance spectrum of standing test for (a) pristine graphene and (b) functional graphene dispersed in THF solution.

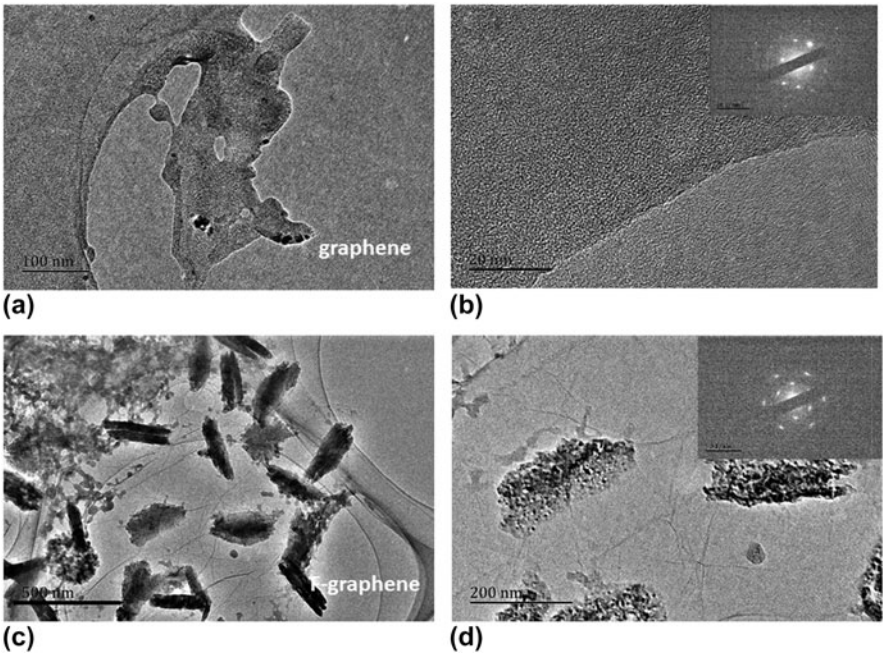


FIG. 5. The TEM images and SAED of (a and b) pristine graphene powders and (c and d) functional graphene powders.

https://doi.org/10.1557/jmr.2016.243 Published online by Cambridge University Press

the thin graphene sheets with few layers as shown in Figs. 5(c) and 5(d). From the selected area electron diffraction (SAED) patterns in Fig. 5(d). It can be inferred that F-graphene is fully exfoliation.[25,26] The TEM image of GO was shown in Fig. S2, the results indicated that the graphene was well oxidized. The SEM image of F-graphene [Fig. 6(b)] is much smoother than the former one and graphene oxide (Fig. S3). One should note that the exfoliation and functionalization of graphene can provide a completely contact with the donor in BHJ structure.

To demonstrate the potential application of the F-graphene in photovoltaic cells, we firstly carried out the P3HT:F-graphene BHJ blend in photodetector with a sandwich structure of ITO/P3HT:F-graphene/Ag at different ratios. The photoelectric response properties in more detail and detect potential application in photoelectronic detection field. We have performed further experiments of photodetector under illumination, shown in Fig. 7. In Fig. 7(a), only chaotic current response can be found that when the proportion of P3HT and F-graphene is 4:1. Moreover, as the ratio increases to 6:1 and 8:1 [Figs. 7(b) and 7(c)], the obvious phenomenon of photoelectric switch is to be found with the current relaxation. However, with the extension of testing time, the relaxation

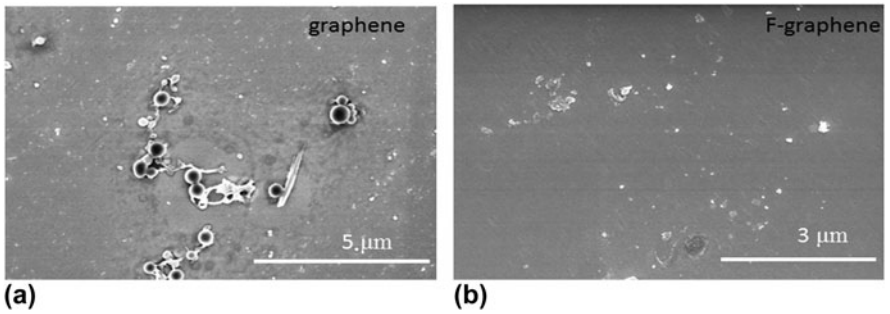


FIG. 6. The SEM images of (a) pristine graphene film and (b) functional graphene film.

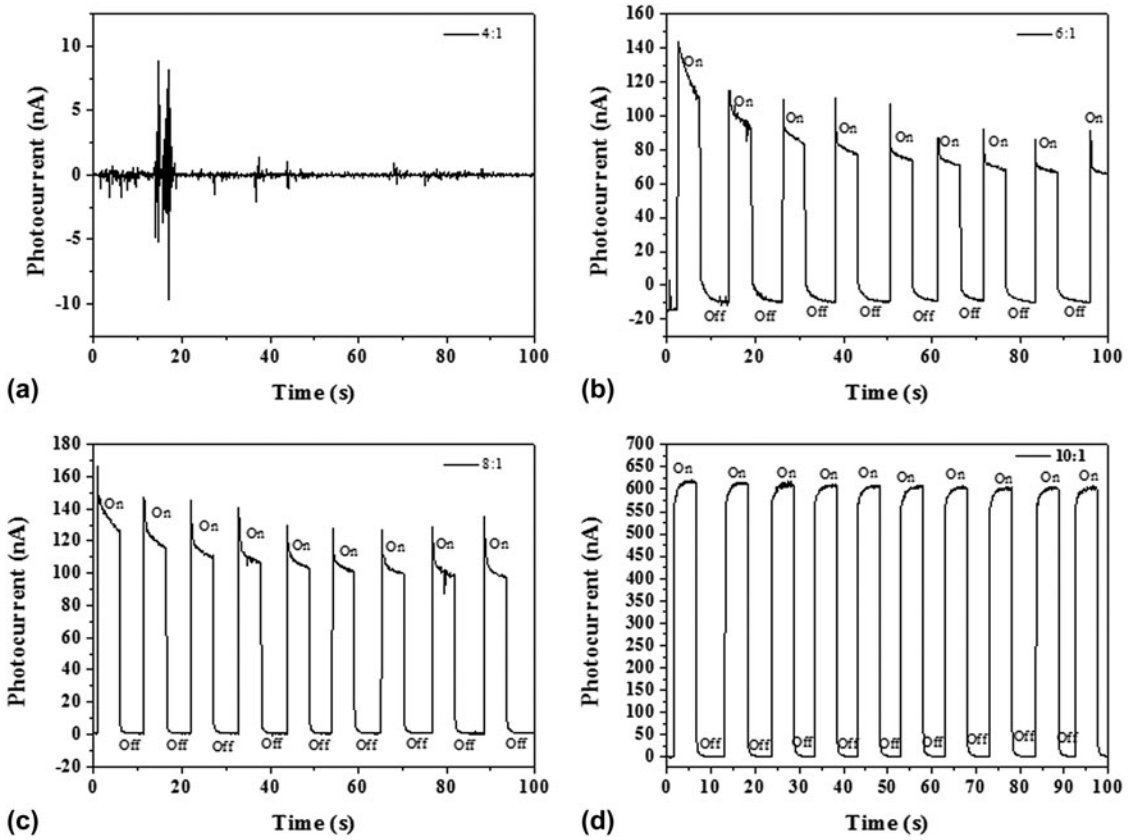


FIG. 7. Photoresponse of P3HT:F-graphene-based photodetectors with different ratios. The output signal of photocurrent under alternating light on and light off, where the entire device was illuminated by 150 W Xe lamp irradiation. (a) P3HT:F-graphene = 4:1, (b) P3HT:F-graphene = 6:1, (c) P3HT:F-graphene = 8:1, (d) P3HT:F-graphene = 10:1.

https://doi.org/10.1557/jmr.2016.243 Published online by Cambridge University Press

phenomenon could be more obvious, and there will be certain photocurrent attenuation. Gratifyingly, when the ratio grows up to 10:1, the BHJ device shows an outstanding photodetector performance while the photoresponse is steady, prompt, and reproducible during repeated on/off cycles of visible light illumination. On the other hand, the P3HT:F-graphene blend demonstrates an obvious photovoltaic effect, which means the F-graphene could play as an acceptor in BHJ. XRD was conducted to analyze the existence of F-graphene in BHJ. As shown in Fig. S3, the diffraction peak at 6.2 and 22.3° is assigned to the (100) diffraction of P3HT and characteristic peak of F-graphene, respectively. The result confirms the existence of F-graphene in BHJ.

As schematically shown in Fig. 8(a), organic photovoltaic cells with the structure of ITO/ZnO/P3HT:F-graphene/MoO_3/Ag were fabricated. A postfabrication annealing of the P3HT:F-graphene BHJ active layer was carried out at 150 °C for 10 min under N_2, which does not only improve the morphology of the P3HT matrix but more importantly removes the residual functional groups in the graphene sheet to increase the conjugation length for enhancing the charge transport mobility. Figure 8(b) gives the energy level diagram for the P3HT:F-graphene device. The AFM was measured to investigate the morphology of BHJ layer. As shown in Fig. 8(c), the P3HT:F-graphene surface shows the homogeneous morphology, while the P3HT:GO (Fig. S5) presents an aggregation of GO attributing to the low dispersibility of GO in THF. To confirm existence of F-graphene in BHJ, the XPS spectra of P3HT:graphene (10:1) and P3HT:F-graphene (10:1) films were measured. As shown in Fig. S6(a), P3HT:F-graphene presents a sharp O1*s* peak in the spectra while P3HT:graphene shows rare O1*s* peak corresponding with the XPS of graphene and F-graphene. Because the content of N element in BHJ is rare, N element is hard to be detected. However, P3HT:F-graphene still presents a weak peak of N1*s* compared with P3HT:graphene film. The results show that F-graphene is existent in BHJ. Figure 8(d) shows the *J*–*V* curves for P3HT:F-graphene BHJ photovoltaic cells. As expected, the photovoltaic characteristics point out that the device with a ratio of 10:1(P3HT:F-graphene) shows a well photovoltaic performance exhibiting an open-circuit voltage (V_{oc}) of 0.61 V, short-circuit current density (J_{sc}) of 5.95 mA/cm^2, fill factor of 0.52, and PCE (η) of 1.9%. Despite these promising results, the efficiency of the graphene-based OSC devices is still lower than the fullerene-based devices (over 10%). And the energy level differences of the donor and acceptor materials of the graphene-based system indeed prove to not match as well as in the polymer-fullerene BHJ. Therefore, extensive research in the design of new graphene-based acceptor with tailored band gap and their corresponding polymer donors is urgently needed.

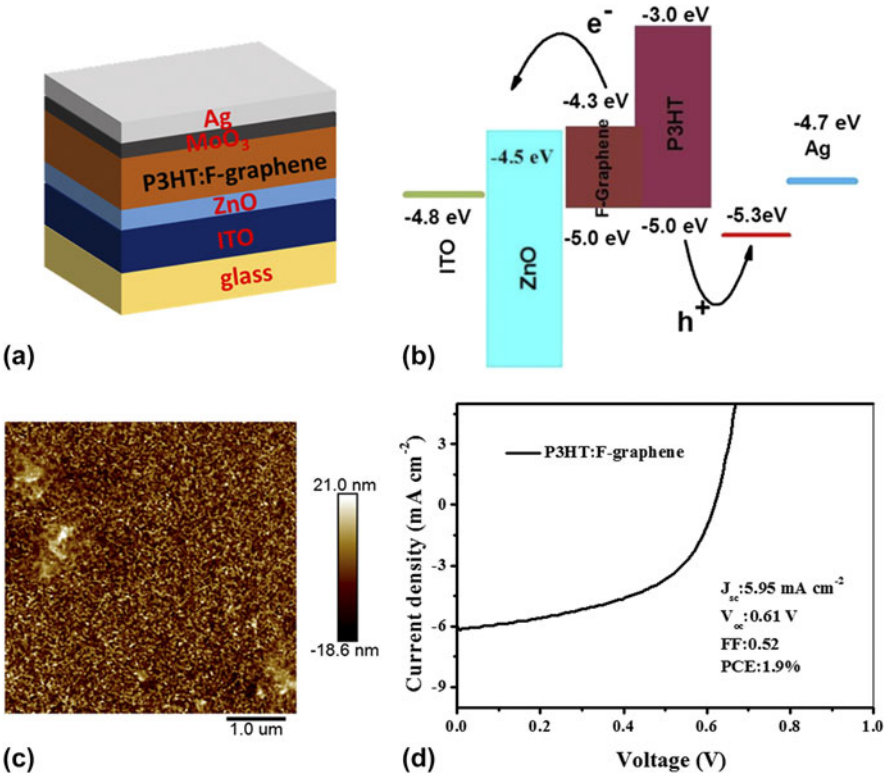


FIG. 8. (a) Schematic and (b) energy level diagram of ITO/ZnO/P3HT:F-graphene/MoO_3/Ag photovoltaic device. (c) Tapping model of AFM height image of ITO/ZnO/P3HT:F-graphene surface. (d) Current voltage characteristics of the photovoltaic devices using P3HT:F-graphene as the active layer which were under the illumination of AM1.5G, 100 mW/cm^2.

https://doi.org/10.1557/jmr.2016.243 Published online by Cambridge University Press

IV. CONCLUSIONS

A novel solution-processed functional graphene was synthesized through a simple method. And the F-graphene showed good solubility in the normal organic solvent. The photovoltaic devices were fabricated with a BHJ structure of ITO/ZnO/P3HT:F-graphene/MoO_3/Ag. The highest PCEs of the devices using P3HT:F-graphene was 1.9%, with a composite ratio of 10:1. The sufficient photovoltaic performance of F-graphene, without any optimization, renders this novel graphene-based material as an alternative electron acceptor for OSC devices. It can be easily anticipated that its performance would be enhanced following the proper optimization.

ACKNOWLEDGMENTS

This subject was financially supported by Natural Science Research Projects Funded of Anhui Colleges and Universities (KJ2015A224) and the Scientific Research Fund of Anhui Province Education Department (KJ2010B104).

REFERENCES

1. G. Yu, J. Gao, J. Hummelen, F. Wudl, and A. Heeger: Polymer photovoltaic cells: Enhanced efficiencies via a network of internal donor–acceptor heterojunctions. *Science* **270**(5243), 1789 (1995).
2. A.J. Heeger: 25th anniversary article: Bulk heterojunction solar cells: Understanding the mechanism of operation. *Adv. Mater.* **26**(1), 10 (2014).
3. F. Guo, X. Zhu, K. Forberich, J. Krantz, T. Stubhan, M. Salinas, M. Halik, S. Spallek, B. Butz, E. Spiecker, T. Ameri, N. Li, P. Kubis, D.M. Guldi, G.J. Matt, and C.J. Brabec: ITO-Free and fully solution-processed semitransparent organic solar cells with high fill factors. *Adv. Energy Mater.* **3**(8), 1062 (2013).
4. L. Dou, J. You, Z. Hong, Z. Xu, G. Li, R.A. Street, and Y. Yang: 25th anniversary article: A decade of organic/polymeric photovoltaic research. *Adv. Mater.* **25**(46), 6642 (2013).
5. H-L. Yip and A.K-Y. Jen: Recent advances in solution-processed interfacial materials for efficient and stable polymer solar cells. *Energy Environ. Sci.* **5**(3), 5994 (2012).
6. C-C. Chen, L. Dou, J. Gao, W-H. Chang, G. Li, and Y. Yang: High-performance semi-transparent polymer solar cells possessing tandem structures. *Energy Environ. Sci.* **6**(9), 2714 (2013).
7. S.H. Park, A. Roy, S. Beaupré, S. Cho, N. Coates, J.S. Moon, D. Moses, M. Leclerc, K. Lee, and A.J. Heeger: Bulk heterojunction solar cells with internal quantum efficiency approaching 100%. *Nat. Photonics* **3**(5), 297 (2009).
8. W. Cai, X. Gong, and Y. Cao: Polymer solar cells: Recent development and possible routes for improvement in the performance. *Sol. Energy Mater. Sol. Cells* **94**(2), 114 (2010).
9. L. Lu, T. Zheng, Q. Wu, A.M. Schneider, D. Zhao, and L. Yu: Recent advances in bulk heterojunction polymer solar cells. *Chem. Rev.* **115**(23), 12666 (2015).
10. H. Hoppe and N.S. Sariciftci: Morphology of polymer/fullerene bulk heterojunction solar cells. *J. Mater. Chem.* **16**(1), 45 (2006).
11. Y. Zhou, T. Kurosawa, W. Ma, Y. Guo, L. Fang, K. Vandewal, Y. Diao, C. Wang, Q. Yan, and J. Reinspach: High performance all-polymer solar cell via polymer side-chain engineering. *Adv. Mater.* **26**(22), 3767 (2014).
12. N. Zhou, H. Lin, S.J. Lou, X. Yu, P. Guo, E.F. Manley, S. Loser, P. Hartnett, H. Huang, and M.R. Wasielewski: Morphology-performance relationships in high-efficiency all-polymer solar cells. *Adv. Energy Mater.* **4**(3), 1300785 (2014).
13. Y. Wang, S.W. Tong, X.F. Xu, B. Özyilmaz, and K.P. Loh: Interface engineering of layer-by-layer stacked graphene anodes for high-performance organic solar cells. *Adv. Mater.* **23**(13), 1514 (2011).
14. J. Liu, Y. Xue, Y. Gao, D. Yu, M. Durstock, and L. Dai: Hole and electron extraction layers based on graphene oxide derivatives for high-performance bulk heterojunction solar cells. *Adv. Mater.* **24**(17), 2228 (2012).
15. Z. Yin, J. Zhu, Q. He, X. Cao, C. Tan, H. Chen, Q. Yan, and H. Zhang: Graphene-based materials for solar cell applications. *Adv. Energy Mater.* **4**(1), 1300574 (2014).
16. Z. Zhu, J. Ma, Z. Wang, C. Mu, Z. Fan, L. Du, Y. Bai, L. Fan, H. Yan, and D.L. Phillips: Efficiency enhancement of perovskite solar cells through fast electron extraction: The role of graphene quantum dots. *J. Am. Chem. Soc.* **136**(10), 3760 (2014).
17. D. Yu, Y. Yang, M. Durstock, J-B. Baek, and L. Dai: Soluble P3HT-grafted graphene for efficient bilayer–heterojunction photovoltaic devices. *ACS Nano* **4**(10), 5633 (2010).
18. D. Yu, K. Park, M. Durstock, and L. Dai: Fullerene-grafted graphene for efficient bulk heterojunction polymer photovoltaic devices. *J. Phys. Chem. Lett.* **2**(10), 1113 (2011).
19. Q. Liu, Z. Liu, X. Zhang, L. Yang, N. Zhang, G. Pan, S. Yin, Y. Chen, and J. Wei: Polymer photovoltaic cells based on solution-processable graphene and P3HT. *Adv. Funct. Mater.* **19**(6), 894 (2009).
20. W.S. Hummers, Jr and R.E. Offeman: Preparation of graphitic oxide. *J. Am. Chem. Soc.* **80**(6), 1339 (1958).
21. Y. Sun, J.H. Seo, C.J. Takacs, J. Seifter, and A.J. Heeger: Inverted polymer solar cells integrated with a low-temperature-annealed sol–gel-derived ZnO film as an electron transport layer. *Adv. Mater.* **23**(14), 1679 (2011).
22. P.V. Kumar, N.M. Bardhan, S. Tongay, J. Wu, A.M. Belcher, and J.C. Grossman: Scalable enhancement of graphene oxide properties by thermally driven phase transformation. *Nat. Chem.* **6**(2), 151 (2014).
23. F. Liu, S. Song, D. Xue, and H. Zhang: Folded structured graphene paper for high performance electrode materials. *Adv. Mater.* **24**(8), 1089 (2012).
24. Y. Wang, Y. Li, L. Tang, J. Lu, and J. Li: Application of graphene-modified electrode for selective detection of dopamine. *Electrochem. Commun.* **11**(4), 889 (2009).
25. P.Y. Huang, C.S. Ruiz-Vargas, A.M. van der Zande, W.S. Whitney, M.P. Levendorf, J.W. Kevek, S. Garg, J.S. Alden, C.J. Hustedt, and Y. Zhu: Grains and grain boundaries in single-layer graphene atomic patchwork quilts. *Nature* **469**(7330), 389 (2011).
26. Z. Peng, F. Somodi, S. Helveg, C. Kisielowski, P. Specht, and A.T. Bell: High-resolution in situ and ex situ TEM studies on graphene formation and growth on Pt nanoparticles. *J. Catal.* **286**, 22 (2012).

Supplementary Material

To view supplementary material for this article, please visit http://dx.doi.org/10.1557/jmr.2016.243.

https://doi.org/10.1557/jmr.2016.243 Published online by Cambridge University Press